Journal of Biomedical Optics 5(2), 206–213 (April 2000)

Study of near infrared technology for intracranial hematoma detection

Quan Zhang
Hongyan Ma
Shoko Nioka
Britton Chance
Department of Biochemistry and Biophysics
University of Pennsylvania
Philadelphia, Pennsylvania 19104-6089

Abstract. Although intracranial hematoma detection only requires the continuous wave technique of near infrared spectroscopy (NIRS), previous studies have shown that there are still some problems in obtaining very accurate, reliable hematoma detection. Several of the most important limitations of NIR technology for hematoma detection such as the dynamic range of detection, hair absorption, optical contact, layered structure of the head, and depth of detection are reported in this article. A pulsed light source of variable intensity was designed and studied in order to overcome hair absorption and to increase the dynamic range and depth of detection. An adaptive elastic optical probe was made to improve the optical contact and decrease contact noise. A new microcontroller operated portable hematoma detector was developed. Due to the layered structure of the human head, simulation on a layered medium was analyzed experimentally. Model inhomogeneity tests and animal hematoma tests showed the effectiveness of the improved hematoma detector for intracranial hematoma detection.
[S1083-3668(00)01302-2]

Keywords: intracranial hematomas; near infrared spectroscopy; continuous wave.

Paper JBO-42004 received Aug. 31, 1999; revised manuscript received Feb. 29, 2000; accepted for publication Mar. 10, 2000.

1 Introduction

Research in the field of near infrared spectroscopy (NIRS) for measuring tissue properties dates back to Millikan,[1] who first developed a dual wavelength muscle oximeter, and Jobsis,[2] who was the first to note that the spectral absorption of both hemoglobin and cytochrome aa_3 could be observed *in vivo* with near infrared transillumination. This method's noninvasive, economical, and easy-to-use characteristics led to extensive interest in studies of its potential clinical application, and it has been found to be a very useful technique in tumor diagnosis, brain function studies, etc.[3–14] Intracranial hematoma detection is one of the most basic and important applications of near infrared spectroscopy.

Intracranial hematoma is a pervasive problem in clinical settings dealing with traumatic brain injury. Expanding hematomas cause damage to the brain by increasing intracranial pressure and by causing a shift of the brain, compressing the brainstem structures. Significant disability or death can occur if the presence of a traumatic intracranial hematoma is not promptly identified and treated. Early diagnosis prior to neurological deterioration is the key to successful surgical treatment.

The basic principle of hematoma detection with NIRS is that water absorption in the near infrared range is relatively small and hemoglobin contributes to most of the tissue absorption; extravascular blood absorbs NIR light more than normal brain tissue since there is a greater concentration of hemoglobin in an acute hematoma. By comparing the reflected and diffusing optical signal I from the suspicious hematoma side and I_0 from the healthy side or from a standard model, the optical density (OD) can be calculated:

$$\mathrm{OD} = \log(I_0 / I). \tag{1}$$

Then intracranial hematoma can be detected by comparing the OD with the detection threshold. Thus, continuous wave spectroscopy (CWS) using a single wavelength spectrophotometer is capable of detecting hematomas. Since intracranial hematomas after head injury are often bilateral, using I_0 from a standard calibration model is recommended. The disadvantage of this simple detection criterion is that, when hematomas vary too much in depth, Eq. (1) will not be valid for the diagnosis. But even though previous research[15,16] shows that NIRS is feasible in the initial triage for head injured patients immediately after injury and for monitoring in the ICU for delayed or recurrent hematomas. In these situations, standard computed tomography (CT) scanning may not be immediately available, or it requires that the patients, many of whom are critically ill, be taken out of the intensive care unit. NIRS instrumentation can be made portable and ambulatory where it is more suitable for these applications.

Although hematoma detection only requires the basic technique of NIRS, previous studies show that there continue to be limitations for accurate and reliable hematoma detection. Most of these limitations are also basic problems for other applications of NIRS. These limitations include the dynamic range of detection, scalp hematomas and hair absorption, deep

Address all correspondence to Quan Zhang, PhD, NMR Center, MGH Building 149, 13th Street, Charlestown, MA 02129. Tel: 617-726-4024; Fax: 617-726-7422; E-mail: qzhang@nmr.mgh.harvard.edu

1083-3668/2000/$15.00 © 2000 SPIE

intracranial hematoma detection, optical contact, and layered structure of human heads, etc.

Concentrating on improving the NIR technology for intracranial hematoma detection, this article consists of three studies. First, the current limitations in intracranial hematoma detection were studied and our solutions to the problems are given. Second, based on the analysis of the current limitation, a pulsed light source of variable intensity was designed in order to overcome hair absorption and to increase the dynamic range and depth of detection; an adaptive elastic optical probe was made to improve the optical contact and decrease contact noise; and a new portable micro-controller operated hematoma detection instrument was developed. Third, using this instrument we performed a model simulation study which includes a model heterogeneity test and simulation of the effects of the layered structure of the head; an animal hematoma test was carried out to demonstrate its effectiveness for intracranial hematoma detection. These efforts were made to go a step further in removing the limitations to successful hematoma detection.

2 Study of the Current Limitations in Intracranial Hematoma Detection

2.1 Dynamic Range of Detection

Different optical properties of tissues in subjects and different source detector separations result in a large range of signals being obtained. We performed a simulation study based on the diffusion equation and semi-infinite boundary condition to examine the dynamic range of the reflectance signal. With a fixed incident light intensity, if the separation between the source and the detector varies from 1.5 to larger than 3 cm, or when the tissue absorption coefficient changes from 0.06 to 0.315 cm^{-1} or more, the simulation result shows that the dynamic range of detection would be more than 80 dB. This requires a complex gain control circuit and is not recommended for a portable instrument. One of the alternative solutions to this problem is to make a light source with adjustable intensity.

2.2 Scalp Hematomas and Hair Absorption

Scalp hematomas and hair absorption are potential problems in trauma patients that could confound the NIRS measurements. Even after hair removal, the hair foot in the skin may still cause significant photon loss and result in a small signal and a low signal-to-noise ratio. In order to overcome this problem high incident light intensity is needed. However, if a laser is used as the light source, the maximum permissible exposure (MPE) according to FDA regulations limit the maximum power transmitted to the skin to only 2–5 mW/mm^2 for a wavelength of 700–900 nm and exposure of 10 s or more.[17] A light emitting diode (LED) source of high light intensity can be considered for use when faced with this limitation.

2.3 Deep Intracranial Hematoma Detection

According to position, difference intracranial hematoma can be divided into epidural, subdural, and intracerebral types. The exact depth of the brain that can be examined by NIRS is still controversial. Previous studies show that deep intraparenchymal hematomas cannot be detected with the NIRS probes that are currently used. In order to get information from deep inside the brain, according to the ''banana shape'' distribution of reflecting diffusing light, the separation between the source and detector must be increased. Since the reflectance detected decreases almost exponentially, when the source–detector separation is more than 4 cm, a satisfying signal-to-noise ratio is hard to obtain. One solution to this problem is to increase the source's light intensity.

2.4 Optical Contact

The photon current will have significant and unstable loss at the contact boundary between the optical probe and the tissue surface. Poor optical contact results in noise, false signals, and inconsistent readings. Since the surface of the head is usually not flat, a hard probe will often fail to make close contact with the skin. A flexible optical probe that is adaptive to the skins surface is a better solution.

2.5 Layered Structure of the Human Head

Several layers exist extracerebrally, including skin, skull, and cerebrospinal fluid. Photon migration through a layered medium is a problem that draws a lot of interest from physicists and engineers. Many studies have been performed to give an analytical, numerical, or empirical solution to this problem,[18–23] and usually an empirical scattering coefficient is assumed in the expression. One clinical study suggested that, with optode separations of less than 4 cm, extracerebral tissues might contribute to the major portion of the NIRS signal.[16] Another study using selective injection of indocyanine green into the internal and external carotid arteries shows that when the source–detector separation is less than 3 cm, the contribution of the internal carotid signal is proportional to the distance of the separation, when it is between 3 and 7 cm, the external carotid signal is constant.[16] Moreover, each region of the skull has varying tissue layer thicknesses that may influence the NIRS signal. In this article we first simulate a solid model and then apply the result to a piglet test.

3 New Intracranial Hematoma Detection Instrument

3.1 Pulsed Light Source of Variable Intensity

3.1.1 *Light source*

A LED was selected to be the light source for hematoma detection. One of the most important reasons for choosing a LED is that there are no strict FDA limitations for the radiation power, thus the light intensity can be increased to overcome the difficulty of hair absorption and deep hematoma detection. Compared with quantitative measurement of oxygen saturation or other applications, the incident light for hematoma detection does not require as sharp a spectrum distribution as does the laser. Also a LED is more economical and easier to use than a laser diode.

3.1.2 *Wavelength*

A wavelength of 805 nm is suitable for hematoma detection since it is very close to the isosbestic wavelength of oxyhemoglobin and deoxyhemoglobin absorption, and the signal detected will not be affected by differences in oxygen satura-

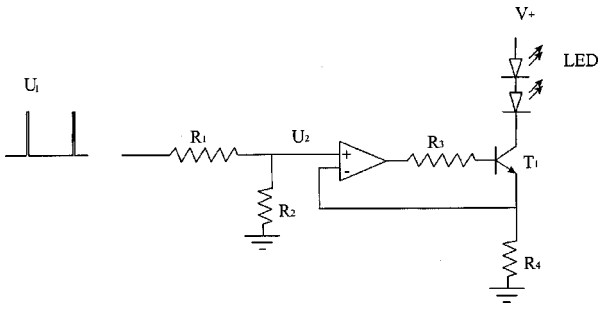

Fig. 1 Pulsed source of a variable light intensity driving circuit.

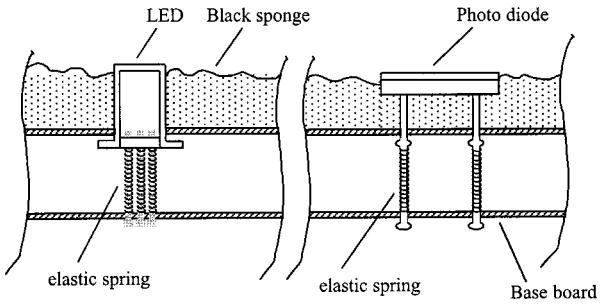

Fig. 2 Structure of the elastic optical probe. The LED and photodiode are mounted on the baseboard, and a black sponge is used to prevent leakage of light from the source to the detector. Springs mounted under the source and detector make the position of the LED and photodiode flexible. When pressed to the head, they are adaptive for close surface contact.

tion in blood. The LED chosen is from Opto Technology, Inc., and operates at 805 nm, with a typical output of 3.5 mW at a current of 20 mA.

3.1.3 *Circuit description*

A pulsed source of variable light intensity was designed. Figure 1 shows a diagram of this circuit. The basis of the circuit is a voltage–current converter, working as

$$I_{\mathrm{LED}} \approx U_1 R_1 / (R_1 + R_2) / R_4 . \tag{2}$$

Negative feedback in this circuit is used to stabilize the current through the LED since the emission power of a LED is usually linear to its current. Also, because of this feedback, the current going through the LED is independent of differences in individual LEDs, which is convenient for replacement in case of damage or failure. Control voltage U_1 may come either from a digital-to-analog converter (DAC) or a voltage divider consisting of resistor networks and switches. The resistance network R_1 and R_2 is for adjusting the input voltage range since direct current control voltage U_2 is usually small and the input voltage U_1 usually has a large dynamical range. If U_1 comes from the DAC, this method is helpful for using the whole DAC output range to improve control accuracy. By controlling U_1 the incident light intensity can be easily adjusted according to different detection situations. For example, $U_1 = 0-10\,\mathrm{V}$, $R_1 = 16\,\mathrm{K}$, $R_2 = 1\,\mathrm{K}$, $R_3 = 4.2\,\mathrm{K}$, and $R_4 = 5\,\Omega$, $T1$ as the 2N2222 transistor, current through the LED will be adjustable in the range of 0–110 mA.

3.1.4 *Efforts to increase light intensity*

One way to overcome hair absorption and to detect deep hematoma is to increase the incident light intensity. The most important factor limiting high LED output power is temperature. For instance, if our LED temperature is less than 125°C, the driving current can go as high as 170 mA and the output is still linear to the current. By using a pulse modulated driving current, the incident light intensity can be increased significantly.

Another method by which to increase light intensity is to put two LEDs in series and let them emit simultaneously; the light intensity will then be doubled. To reach the same light intensity, use of two LEDs in series is safer since the peak current required is only about half that using only one LED. Present technology can easily integrate two LEDs into one TO-18 package with a shell diameter of 4.5 mm, and the distance between two emitting parts inside is about 0.8 mm, so detected diffusing light going through different paths of tissue is not a concern.

With two LEDs in series working at a pulse peak current of 100 mA, experiments showed that a 20 dB signal-to-noise ratio can be acquired at 4 cm source detector separation on a model of $\mu a = 0.13\,\mathrm{cm}^{-1}$ and $\mu s' = 13\,\mathrm{cm}^{-1}$. If a good detection method like coherent averaging is used, the signal-to-noise ratio can go even higher. On normal adult subjects, the detection separation can extend 6 cm or more on the forehead using this method.

Since the output power of the light source can be accurately controlled after calibration of the linear relationship between the driving current and the output light level, we can adjust the incident light intensity during the measurement and then correct this initial amplitude change in the subsequent calculation of the OD values. For example, if tissue absorption is high and we need to double the incident light intensity to get the reflectance signal I with a reasonable signal-to-noise ratio, when we calculate the OD we can correct this light intensity change by a factor of 0.5, that is, instead of using $\log(I_0/I)$, the corrected OD value should be OD $= \log(I_0/0.5I)$.

3.2 Adaptive Elastic Optical Probe

The structure of the elastic optical probe is shown in Figure 2. The LED and photodiode are mounted on the baseboard, which can be curved a little to fit the shape of a human head. A black sponge is used to prevent leakage of light from the source to the detector. The key to making the probe elastic is springs mounted under the source and detector, thus making the position of the LED and photodiode flexible. When pressed to the head, they are adaptive for close contact with the surface.

The performance of this probe was tested on the solid model and on the forehead of normal subjects to see the repeatability of the results. The fluctuation was about 10% of the detected signal. The flexible probe improves optical contact, but we cannot say that it totally solves the contact problem; for example, movement of the skin also results in signal instability.

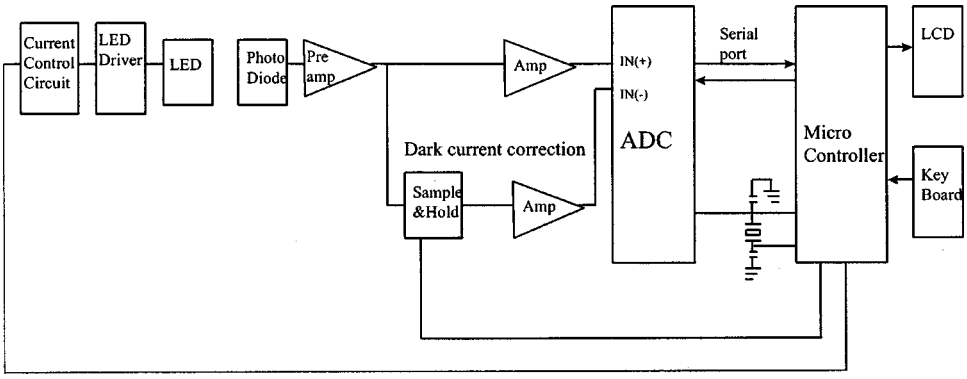

Fig. 3 Block diagram of the portable hematoma detector.

3.3 Microcontroller Operated Portable Hematoma Detector

3.3.1 *Hardware*

A block diagram of the portable hematoma detector is displayed in Figure 3. A pulsed driving circuit drives the LED light source. The current control circuit can either be a DAC or a voltage divider. According to the command given by the microcontroller, it generates different control voltages to adjust the light intensity. During the light pulse off period, the detected signal, which is actually ''dark current'' or background light, is sampled and held for dark signal correction. During the light pulse on period, the reflected diffusing light signal detected by the photodiode is amplified and also input into the ADC. Since the ADC is working in a differential input state, the dark voltage is subtracted from the light voltage, the corrected signal is amplified inside the ADC, then digitized, and finally transported to the microcontroller. Although alternatively the dark signal can also go through the same channel as the light signal and be memorized and subtracted in the microcontroller, the former hardware subtraction method is better in rejecting background light and expanding the dynamic range of detection, since only the difference between the light signal and dark signal is amplified and processed inside the ADC. The ADC communicates with the microcontroller through a serial port. The microcontroller is in charge of the whole operation, which includes acquiring the signal, calculating the OD, adjusting the incident light intensity, and communicating with the operator. The LCD is used for displaying measurement results and operating information. Keys are used as an input path to get information from the operator.

3.3.2 *Software*

Figure 4 is the main flow chart diagram of the software. When the side with a suspected hematoma cannot be clearly distinguished from the healthy one, a calibration model should be used to get I_0. Since it is very hard for the microcontroller to perform a logarithm calculation, the OD calculation is completed first by division then changed to OD using a look-up table. Usually two OD thresholds are set for hematoma identification. For example, if the OD between the healthy side of the brain and the injured side of the brain is larger than 0.3 OD, that case is determined as the hematoma occurs; if it is between 0.1 and 0.3 OD, a warning signal is given; if it is less than 0.1 OD, then it is evaluated as having no hematoma. Reference 16 presents some valuable clinical OD data for hematoma detection.

4 Model Simulation Study and Animal Experiment

4.1 Model Heterogeneity Test

A model heterogeneity test was performed to examine the performance of the hematoma detector. The results of the experiment are shown in Figure 5. A solid phantom with μa of about 0.03 cm^{-1} and $\mu s'$ of about 10 cm^{-1} was used to simulate a human brain. Phantoms are made from polyester

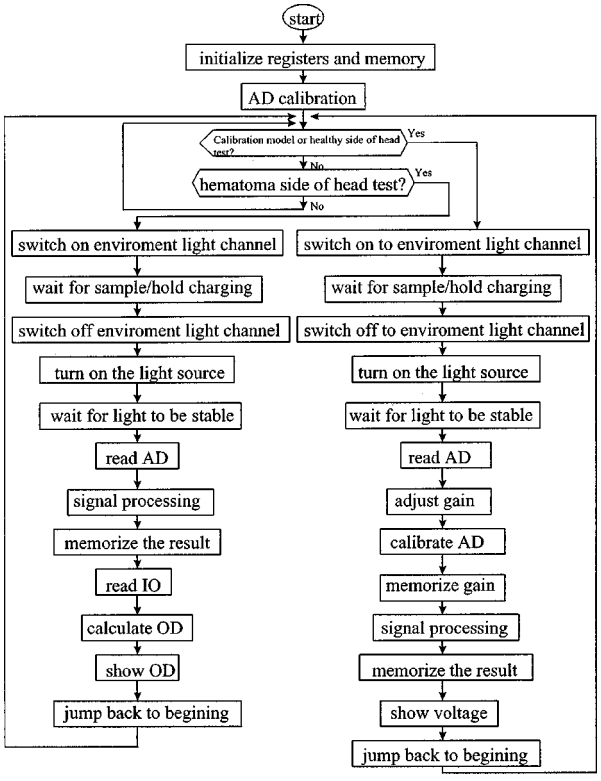

Fig. 4 Main flow chart diagram of the software for the microcontroller operated hematoma detector.

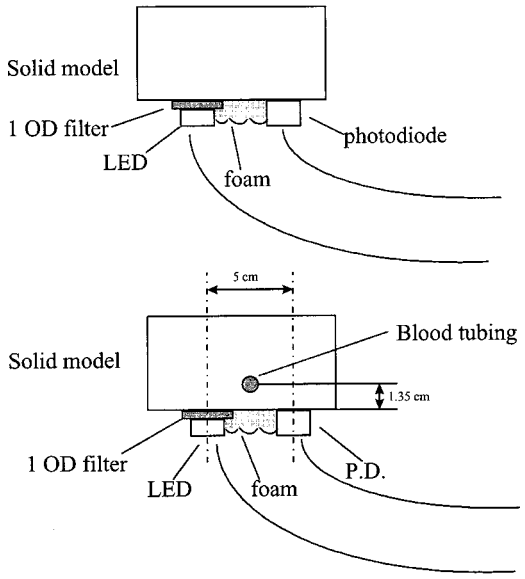

Fig. 5 Model inhomogeneity test.

resin, titanium oxide powder, and India ink of different concentrations. The latter two substances are used to adjust the model's scattering and absorption properties. The optical probe was put on the surface of the phantom. The separation between the source and detector was 5 cm. A 1 OD filter was put between the LED and the phantom to simulate hair or skin absorption. First a control voltage was acquired to simulate the healthy side of the head. Then a hole was made in the phantom 1.35 cm from the surface and a tube containing whole blood was put into it and a simulating hematoma signal was acquired. The OD was calculated to identify the hematoma. In this test the control voltage was 3000 mV and the hematoma voltage 1300 mV, and the calculated optical density was larger than 0.3 OD.

4.2 Experimental Studies of the Layered Medium

Two phantom studies of the layered medium problem were performed, as shown in Figure 6. Two layers of the medium

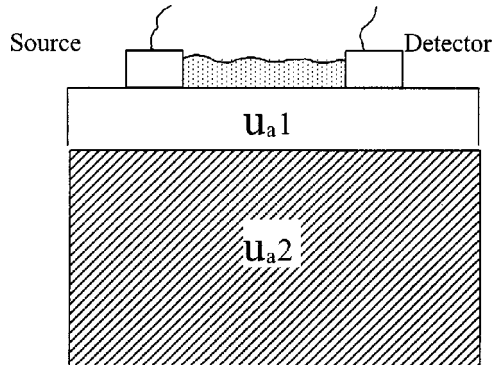

Fig. 6 Phantom studies of the layered medium problem.

with different optical properties were used in this study. The contact boundary between the two layers was made perfectly flat so that there would be no significant loss of light at the boundary. The source and detector were put on the surface of the first layer and the black sponge was used to prevent leakage of light. Signal I acquired from the layered medium was compared with control signal I_0 from a control model to calculate the OD.

In the first study, the relationship among the detection threshold, the depth of the top layer, and the source detector separation as examined. The top layer simulated tissues above the hematoma like skin, skull, etc., with μa_1 of 0.03 cm^{-1} and $\mu s'$ of 13 cm^{-1}. The bottom layer simulated the hematoma, with μa_2 of 0.16 cm^{-1} and $\mu s'$ of 13 cm^{-1}. The thickness of the bottom layer is more than 40 mm. The thickness of the top layer was increased and the reflected light intensity with different source–detector separations was measured. The result is shown in Figure 7.

From the result in Figure 7, it was determined that the OD decreases when the top layer thickness increases. This means the hematoma detection threshold needs to be adjusted according to the depth of the top tissue layer. For example, if the simulated top layer thickness is 5 mm, the source–detector separation is 35 mm and 1.4 OD is used as the threshold for simulated hematoma detection. When the simulated top tissue

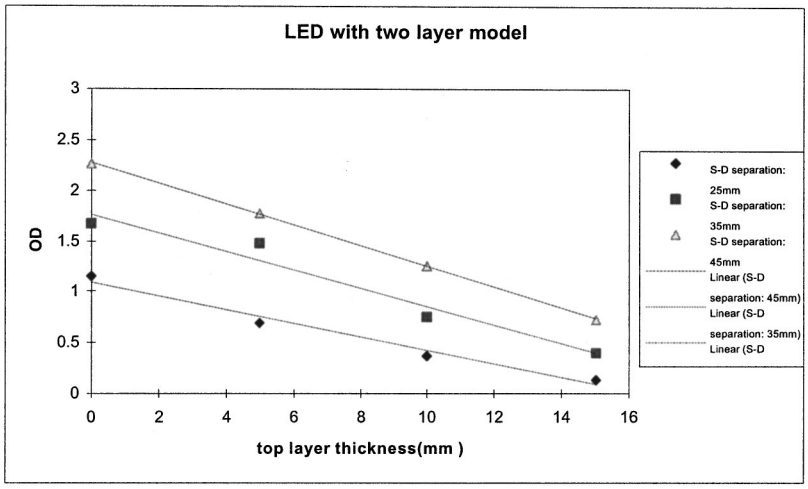

Fig. 7 Phantom simulation result of the relationship among the detection threshold, the depth of the top layer, and the source–detector separation.

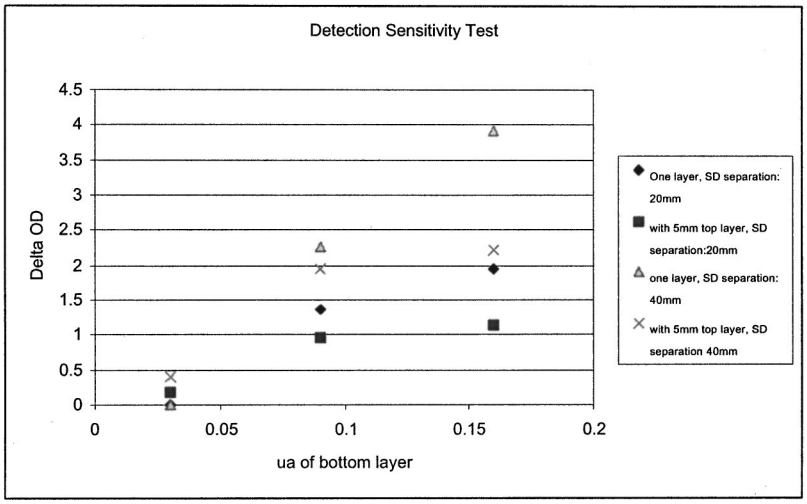

Fig. 8 Phantom simulation result of the sensitivity of the OD change vs the bottom layer absorption change (δ OD/$\delta\,\mu a_2$) for different source–detector separations.

layer thickness increased to 10 mm, the threshold needs to be adjusted to 0.8 OD. Since a small OD threshold is easily affected by noise, this means that the thicker the top tissue layer is, the less sensitive the detection will be. The approximate relationship between OD and top layer thickness in the experiment can be fitted to a linear function. If this is true for all cases, then it means the detection threshold can be adjusted linearly according to top layer thickness. In our experiment the adjustment is around -0.09 OD/mm with 4 cm source–detector separation.

Another conclusion we reach from this experiment is that the larger the source–detector separation is, the more sensitive the detection is. As can be seen from the data, with the same top layer thickness, the larger source–detector separation yields larger OD values. For example, with a 10 mm top layer, the simulated threshold for a 45 mm source–detector separation is 1.3 OD, for a 35 mm separation it is 0.7 OD, and for 25 mm it is 0.4 OD.

In the second experiment, the sensitivity of the OD change versus bottom layer absorption change (δ OD/$\delta\,\mu a_2$) for different source–detector separations was examined. First, measurements were made for different source–detector separations on a one-layer model; its absorption coefficient μa_2 goes from 0.3 to 0.16 cm^{-1}, and μs is 13 cm^{-1}. Subsequently, a 5 mm top layer was added above the model and the same measurements were made on the top layer for different source–detector separations. The optical property of the top layer is $\mu a_1 = 0.03\,\text{cm}^{-1}$ and $\mu s' = 13\,\text{cm}^{-1}$. The results are shown in Figure 8.

From the results in Figure 8, it can be seen that, first, with a fixed source–detector separation, the relationship between OD and μa is not linear. If the concept of the differential pathlength factor (DPF) is used, this can be explained as the DPF not being a constant when the absorption of the bottom layer changes. Second, if there is a less absorbing top layer, the sensitivity (defined as δ OD/$\delta\,\mu a_2$) will decrease. This means the OD change is less sensitive to the bottom absorption coefficient change. In our experiment when the bottom μ_a changes from 0.03 to 0.09 cm^{-1}, the sensitivity decreased 72% when a 5 mm top layer was added on the top (the source–detector separation is 20 mm). Third, the sensitivity (δ OD/$\delta\,\mu a_2$) will increase when the source–detector separation increases. When the separation increases from 20 to 40 mm, the sensitivity increases from 2.3 to 3.6 OD cm (with a 5 mm top layer). These results agree with the clinical study.

4.3 Piglet Hematoma Test

An animal experiment was performed to test the effectiveness of this instrument. The piglet was about 5 days old. A window was made in the skull and an intracranial hematoma was induced by a surgical operation. The hematoma layer is right under the skull and is about 1 mm thick. Blood in blood vessels was washed out by injecting saline solution into the circulation system. Four measurements were made at different positions, shown in Figure 9. The source detector separation was 4 cm, and the LED current for detection was 18.3 mA. The calibration procedure took place on a solid model with

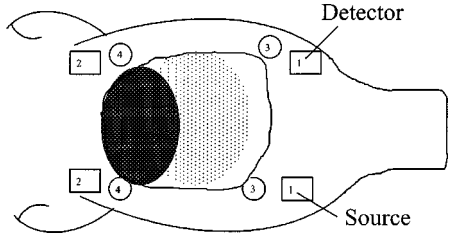

Fig. 9 Piglet hematoma test. The black shaded area is the epidural hematoma. The squares on the left are source and detector positions for the hematoma side and the squares on the right are source and detector positions for the healthy side for the first measurement. The circles on the left are source and detector positions for the hematoma side and the circles on the right are source and detector positions for the healthy side for the second measurement.

Table 1 Piglet hematoma test ($I_0 = 8.8$ V on model of $\mu a = 0.03$ and $\mu s' = 13$).

Position	Healthy side (OD)	Hematoma side (OD)
1	0.29	1.25
2	0.40	1.1

$\mu a = 0.03$ and $\mu s' = 13$, and the signal we got from the calibration was used as I_0 to calculate the OD. The piglet was, dead before the optical measurement. Table 1 shows the results of the measurement.

In the experiment the thickness of the piglet's skin and skull layer is about 3 mm, and the difference between different positions is less than 1 mm. From the phantom study we can see that with a 4 mm source–detector separation and a 3 mm top layer the OD change is approximately 1.8 OD (Figure 8) when the bottom layer absorption changed from 0.03 to 0.16, larger than the OD change of the piglet's hematoma side which is 1.2 OD. This can be explained as, first, the scattering property of the brain tissue is a little different from the simulation model, and, second, in our phantom study the bottom medium is homogeneous with μa of 0.16; in the piglet head the hematoma is a thin membrane of blood, and under the hematoma membrane the brain tissue absorption is still low. The piglet brain was also tested by phase modulated spectroscopy (PMS) and time resolved spectroscopy (TRS) as a reference, and the results showed the μa and $\mu s'$ of the healthy side of the piglet head to be around 0.05 and 8.5 cm^{-1}, and those of the hematoma side to be around 0.08 and 8.5 cm^{-1}. The difference in OD between the healthy side and the hematoma side of the piglet brain is about 0.8 OD. This experiment demonstrated that the hematoma detector is effective for hematoma detection.

5 Conclusion and Discussion

The significance of this study is twofold. First, we try to solve the problems using the current NIRS method for hematoma detection. Second, since many of the problems of hematoma detection (e.g., hair absorption, optical contact, layered medium) are also common in other applications of NIRS (e.g., imaging and quantitative measurement of the tissue's optical properties), we hope our efforts can also be of some help for these applications.

A pulsed source with variable light intensity was designed to overcome the problem of hair absorption and to increase the dynamical range and depth of detection. An adaptive elastic optical probe was created to improve the optical contact and decrease contact noise; a new microcontroller operated portable hematoma detector was developed; model inhomogeneity tests and animal hematoma tests showed both are effective for intracranial hematoma detection. A phantom study showed the hematoma detection OD threshold needs to be adjusted according to the depth of the top tissue layer, and the detection threshold can be adjusted approximately by top layer thickness using a linear function. A larger source–detector separation should have a larger detection OD threshold, and this should be more robust in resisting detection noise. The sensitivity of the OD change versus the bottom layer absorption change (δ OD/δ μa_2) increases when the source–detector separation increases. When there is a top layer with less absorption, the OD change will be less sensitive to the bottom absorption coefficient change. These simulations and experiments can help to correct the effects of the top layer. More clinical study is needed to get empirical constants to correct for the effect of skin, skull, and other top layer tissue effects. This work was done in order to go a step further in improving current NIRS instrumentation and methods for more accurate hematoma detection.

An analytical or numerical solution of photon migration through a layered medium is needed for an accurate description of photon migration through a layered medium. For example, in Ref. 20, an expression was derived on the basis of a two-layered random-walk lattice model:

$$I(\rho) = \frac{1}{4\pi\rho^2}\{\sqrt{6\mu_1}\exp(-\rho\sqrt{\mu_1}) + \sqrt{6\mu_2} \times \exp[-\rho\sqrt{\mu_2} - m(\mu_1 - \mu_2)]\}, \quad (3)$$

where ρ is the source–detector separation, $I(\rho)$ is the reflectance intensity; μ_1 and μ_2 are absorption coefficients of the upper and bottom layers, and m is a constant that is proportional to the thickness of a top layer. And

$$\frac{\partial \mathrm{OD}}{\partial \mu a_2} = \frac{\partial \ln(I(\rho)/I_0)}{\partial \mu a_2} = A_0\left(\frac{1 + A_1 h}{1 + A_2\exp(A_3 + A_4 h)}\right), \quad (4)$$

where I_0 is the input light intensity, μa_2 is the absorption coefficient of the bottom layer, h is the top layer thickness, and A_0–A_4 are constants determined from results of the simulation and experiments by curve fitting. When applying these to hematoma detection, simulation and experiments are needed to determine the constants. These equations may be used in the future to get better results in hematoma detection with the NIR method. For example, the simple OD criterion of Eq. (1) cannot compensate for the effects of changes in the depth of the hematoma. That is why the current application of this NIR method for hematoma detection is limited mostly to the initial triage for head injured patients immediately after injury and monitoring in the ICU for delayed or recurrent hematomas, where the depths of the hematoma do not change very much. But with a better equation and more accurate criteria the variance of the depth of the hematoma could be handled by multimeasurements with different source–detector separations and corresponding judging thresholds.

NIRS is suitable for hematoma detection because of its portability and ease of use. If the instrument described in this article were connected to a transmitting unit and it communicated with a center station without wires, an ambulatory long term hematoma monitoring system could be developed, which would be very helpful for identification of delayed and recurrent hematoma.

Acknowledgment

The authors would like to thank Juan for the animal experiments, and also thank Xuhui Ma, Regine Choe, Nirmala Ra-

manujam, Gargi Vishnoi, Lori Pfaff and Vesal Dini for their kind help. This research was supported by Grant No. NS44125.

References

1. G. A. Millikan, ''Experiments on muscle haemoglobin,'' *Proc. R. Soc. London, Ser. A* **123**, 218–224 (1937).
2. F. F. Jobsis, ''Non-invasive infra-red monitoring of cerebral and myocardial oxygen sufficiency and circulatory parameters,'' *Science* **198**, 1264–1267 (1977).
3. A. Villringer and B. Chance, ''Non-invasive optical spectroscopy and imaging of human brain function,'' *Trends Neurosci.* **20**, 435–442 (1997).
4. A. Yodh and B. Chance, ''Spectroscopy and imaging with diffusing light,'' *Phys. Today* March, 34–40 (1995).
5. D. A. Boas, ''Diffuse photon probes of turbid media: Theory and applications,'' Ph.D. thesis, University of Pennsylvania, 1996.
6. B. Chance, Q. Luo, S. Nioka, D. Alsop, and J. Detre, ''Optical investigations of physiology: A study of intrinsic and extrinsic biomedical contrast,'' *Philos. Trans. R. Soc. London, Ser. B* **352**, 707–716 (1997).
7. S. Nioka, Q. Luo, and B. Chance, ''Human brain functional imaging with reflectance CWS,'' in *Oxygen Transport to Tissue*, D. K. Harrison and D. T. Delpy, Eds., Vol. XIX, pp. 237–242, Plenum, New York (1997).
8. B. Chance, K. A. Kang, L. He, H. Liu, and S. Zhou, ''Precision localization of hidden absorbers in body tissues with phased-array optical systems,'' *Rev. Sci. Instrum.* **67**, 4324–4332 (1996).
9. B. Chance, H. Liu, T. Kitai, and Y. Zhang, ''Effects of solutes on optical properties of biological materials: Models, cells, and tissues,'' *Anal. Biochem.* **227**, 351–362 (1995).
10. B. Chance, Z. Zhuang, C. Unah, C. Alter, and L. Lipton, ''Cognition-activated low-frequency modulation of light absorption in human brain,'' *Proc. Natl. Acad. Sci. USA* **90**, 3770–3774 (1993).
11. G. Vishnoi, A. H. Hielscher, et al. ''Phantom model studies on photon migration through fetal head *in utero* using continuous-wave near infra-red spectroscopy,'' *Proc. SPIE* 3597 (1999).
12. B. Chance, ''Optical method,'' *Annu. Rev. Biophys. Biophys. Chem.* **20**, 1–28 (1991).
13. B. Chance, M. Cope, E. Gratton, N. Ramanujam, and B. Trombery, ''Phase measurement of light absorption and scatter in human tissue,'' *Rev. Sci. Instrum.* **69**, 3457–3481 (1998).
14. C. S. Robertson, S. P. Gopinath, and B. Chance, ''Use of near infrared spectroscopy to identify traumatic intracranial hematomas,'' *J. Biomed. Opt.* **2**, 31–41 (1997).
15. C. S. Robertson, S. P. Gopinath, and B. Chance, ''Identifying intracracranial hematomas with near-infrared spectroscopy,'' in Transcranial Cerebral Oximetry, G. Litscher and G. Schwarz. Eds., pp. 131–141, Pabst Science, Berlin (1997).
16. ''American national standard for safe use of lasers,'' Report ANSI Z136.1-1993 American National Standard Institute (1993).
17. T. Shiga, K. Tanabe, Y. Nakase, T. Shiga, and B. Chance, ''Development of a portable tissue oximeter using near infra-red spectroscopy,'' *Med. Biol. Eng. Comput.* **33**, 622–626 (1995).
18. K. Yamamoto, M. Niwayama, L. Lin, T. Shiga, N. Kudo, and M. Takahashi, ''Accurate NIRS measurement of muscle oxygenation by correcting the influence of a subcutaneous fat layer,'' *Proc. SPIE* **3194**, 166–173 (Jan. 1998).
19. M. Niwayama, L. Lin, J. Shao, T. Shiga, N. Kudo, and M. Takahashi, ''Quantitative measurement of muscle oxygenation by NIRS: Analysis of the influences of a subcutaneous fat layer and skin,'' *Proc. SPIE* **3597**, 291–299 (April 1999).
20. A. H. Jielscher, H. Liu, and B. Chance, ''Time-resolved photon emission from layered turbid media,'' *Appl. Opt.* **35**, 719–728 (1996).
21. W. Cui and L. E. Ostrander, ''The relationship of surface reflectance measurements to optical properties of layered biological media,'' *IEEE Trans. Biomed. Eng.* **39**, 194–201 (1992).
22. G. Alexandrakis, R. A. Weersink, and J. T. Bruulsema, ''Estimation of the optical properties of two-layer tissue simulating phantoms from spatially resolved frequency-domain reflectance,'' in *Optical Tomography and Spectroscopy of Tissue III*, B. Chance, R. R. Alfano, and B. J. Tromberg, Eds., *Proc. SPIE*, 155–163 (1999).
23. S. Takatani and M. D. Graham, ''Theoretical analysis of diffuse reflectance from a two-layer tissue model,'' *IEEE Trans. Biomed. Eng.* **26**, 656–664 (1979).